

Supporting Information

Double enhancement of protonation and conjugation in donor-imine-donor covalent organic frameworks for photocatalytic hydrogen evolution

Huan He^{a+}, Rongchen Shen^{a+}, Yuhao Yan^{a+}, Dejun Chen^a, Zhixiong Liu^a, Lei Hao^a, Xin Zhang^{b*}, Peng Zhang^{c*}, Xin Li^{a*}

^a *Institute of Biomass Engineering, Key Laboratory of Energy Plants Resource and Utilization of Ministry of Agriculture and Rural Affairs, Key Laboratory for Biobased Materials and Energy of Ministry of Education, College of Materials and Energy, South China Agricultural University, Guangzhou 510642, China. E-mail: Xinli@scau.edu.cn*

^b *Hubei Key Lab Low Dimens Optoelect Mat & Devices, Hubei University of Arts and Science, Xiangyang 441053, Peoples R China. E-mail: xinzhang@hbuas.edu.cn*

^c *State Centre for International Cooperation on Designer Low-Carbon & Environmental Materials (CDLCEM), School of Materials Science and Engineering, Zhengzhou University, Henan, Zhengzhou, 450001, P. R. China. E-mail: zhangp@zzu.edu.cn*

+ *These authors contributed equally to this work*

1. Experimental section

1.1 Materials

All chemicals and reagents were of analytical grade materials and used as received without further purification. The *o*-DCB (1,2-Dichlorobenzene, 99%), anhydrous *n*-But (*n*-Butanol, 99.4%), Acetic acid (>99.0%), 4,4',4'',4'''-(pyrene-1,3,6,8-tetrayl)tetraben (Py-NH₂, ≥98%), 4,4',4'',4'''-(pyrene-1,3,6,8-tetrayl)tetrabenzaldehyde (Py-CHO, 98%) were purchased from Jilin Chinese Academy of Sciences-Yanshen technology Co. Ltd. The rest of the drugs were purchased from Shanghai BiDe Pharmaceutical Technology Co.

1.2 Characterization

1.2.1 Powder X-ray diffraction (PXRD) analysis

Powder X-ray diffraction data was conducted on a Rigaku and Smartlab diffractometer in reflection geometry operating with a Cu K α anode ($\lambda = 1.54178 \text{ \AA}$) operating at 40 kV and 40 mA. Samples were ground and mounted as loose powders onto a Si sample holder. PXRD patterns were collected from 1 to 30 2θ degrees with a step size of 0.02 degrees and an exposure time of 2 seconds per step.

1.2.2 Fourier transform infrared spectroscopy (FTIR) analyses

Fourier transformed infrared (FTIR) spectra were tested on a Nicolet Avatar 6700 FT-IR spectrometer (Thermo Fisher, America).

1.2.3 Solid-state diffuse reflectance Ultraviolet-visible spectroscopy (UV-DRS) analysis

The UV-vis diffuse reflection spectra (UV-vis DRS) of the powders were carried out on a Shimadzu UV-2600 UV-vis-NIR spectrophotometer.

1.2.4 N₂ Physisorption measurements

N₂ sorption measurements were performed on a volumetric sorption instrument (Autosorb-iQ-MP). Prior to the gas sorption studies of COFs, the samples were dried under a dynamic vacuum ($<10^{-3}$ Torr) at room temperature (RT) followed by heating to 120 °C for 12 h. Using the N₂ adsorption isotherms, the surface areas were calculated over a pressure range $0.01-0.9 = P/P_0$ using Brunauer-Emmett-Teller (BET).

1.2.5 X-ray photoelectron spectroscopy (XPS)

X-ray photoelectron spectroscopy (XPS) data was carried out by a VG ESCALAB250 surface measurement system. The specific condition is that the excitation source: Al K α Ray ($h\nu = 1486.6$ eV), Beam spot: 400 μ m, vacuum degree of the analysis chamber is better than 5.0×10^{-7} mBar, working voltage: 12 kV, filament current: 6 mA, full spectrum scanning: pass energy: 100 eV, step size: 1 eV; Narrow spectrum scanning: the energy is 50 eV, and the step size is 0.1 eV. The narrow spectrum shall be subject to at least 5 times of cyclic signal accumulation (different scanning times for different elements), and the binding energy correction: charge correction shall be conducted with C 1s = 284.80 eV binding energy as the energy standard.

1.2.6 High-resolution transmission electron microscopy (HRTEM) and Scanning electron microscopy (SEM)

Transmission electron microscopy (TEM) images were obtained with a JEOL JEM-2010 electron microscope. Scanning electron microscopy (SEM) was conducted on a Hitachi S-4800 field emission scanning electron microscope.

1.2.7 Electron spin resonance spectroscopy (ESR)

ESR measurements in X-band (microwave frequency ≈ 9.87 GHz) were performed at 293 K by a Bruker EMX CW micro spectrometer equipped with an ER 4119HS-WI high-sensitivity optical resonator with a grid in the front side. The samples were illuminated by a 300 W Xe lamp with 420 nm cut-off filter (LOT Oriel). All the samples were measured under the same conditions (microwave power: 6.74 mW, receiver gain: 2×10^4 , modulation frequency: 100 kHz, modulation amplitude: 3 G, Sweep time: 45 s). g values have been calculated from the resonance field B_0 and the resonance frequency ν using the resonance condition $h\nu = g\beta B_0$.

1.2.8 Electrochemical analysis

The working electrodes was fabricated as follows: 5 mg photocatalyst powder was added into 4 mL ethanol solution containing 20 μ L 0.25% of Nafion under ultrasound for 1 h to obtain a slurry. Then, 0.5 mL of the slurry homogeneously dropped on a FTO glass (2 cm \times 3.5 cm). After being calcined for 1 h in a tube furnace at 150 $^{\circ}$ C (N_2 carrier gas), an electrode was obtained. Electrochemical

impedance spectra (EIS) and transient photocurrent experiments were conducted on a CHI-660e electrochemical workstation (Zahner Elektrik, Germany) with a standard three-electrode system, which employed as-fabricated electrodes as the working electrode, a platinum plate as the counter electrode and Ag/AgCl as the reference electrode. A Xe arc lamp (350 W) with a cut-off filter ($\lambda > 420$ nm) was used as the light source. 0.1 M Na₂SO₄ aqueous solution was used as the electrolyte. Mott-Schottky curves were measured in 0.1 M Na₂SO₄ in water, with a 1000, 1500 and 2000 Hz alternating current potential frequency.

1.3 Photocatalytic hydrogen evolution method and parameters

The photocatalytic water splitting reaction under visible-light irradiation was performed in a 250 mL Pyrex top-irradiation reaction vessel with a stationary temperature at 5 °C, which was connected to a glass closed gas system (Labsolar-6A, Perfect Light). In a typical process, 5 mg of photocatalyst was dispersed in a Pyrex reaction cell with 100 mL 0.1 M ascorbic acid aqueous solution and 3 wt% Pt. The reaction cell was sealed, and then irradiated with a 350 W Xe lamp (PLS-SXE300, Beijing Perfect Light Technology Co., Ltd, $\lambda > 420$ nm) under normal atmospheric pressure. During the photocatalytic reaction, the suspension was continuously stirred. The generated hydrogen was detected by GC-9500 online chromatograph.

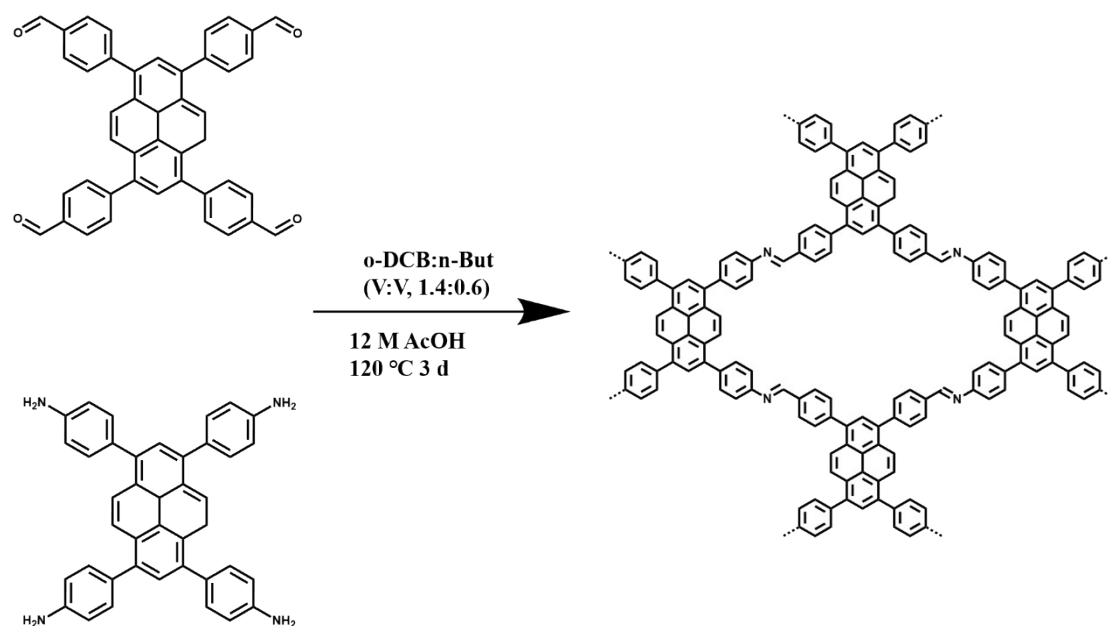
1.4 Calculations Details and Discussions:

The geometry optimizations and characterization of the electronic structures of molecules were obtained at the B3LYP/6-311G* level (Gaussian 9.0 software package). The excited state energies and oscillator strengths from TD-DFT (TD-B3LYP/6-311G*) scrf calculations for the transient species. The implicit solvent model and dispersion correction are also used in the calculation. The distribution of electrons and holes in the electron excitation process was calculated using Multiwfn (version 3.8). The charge density difference map was constructed by the Multiwfn program¹ and Visual Molecular Dynamics and LOL-pi². A structural model of COFs was executed by using the Materials Visualizer module of Materials Studio software following the procedure: The space groups were obtained from the Reticular Chemistry Structure Resource (RCSR). Upon completion of the structural model, an

energetic minimization was performed using the universal force field implemented in the Forcite module. Pawley refinements of the PXRD patterns were done in the Reflex module. The integrated intensities were extracted using Pseudo-Voigt profile. The unit cell parameters a , b , c , FWHM parameters U , V , W , profile parameters NA , NB , and zero point were refined. The background was refined with 20th order polynomial. Simulated PXRD patterns were generated based on the optimized structures using Reflex module.

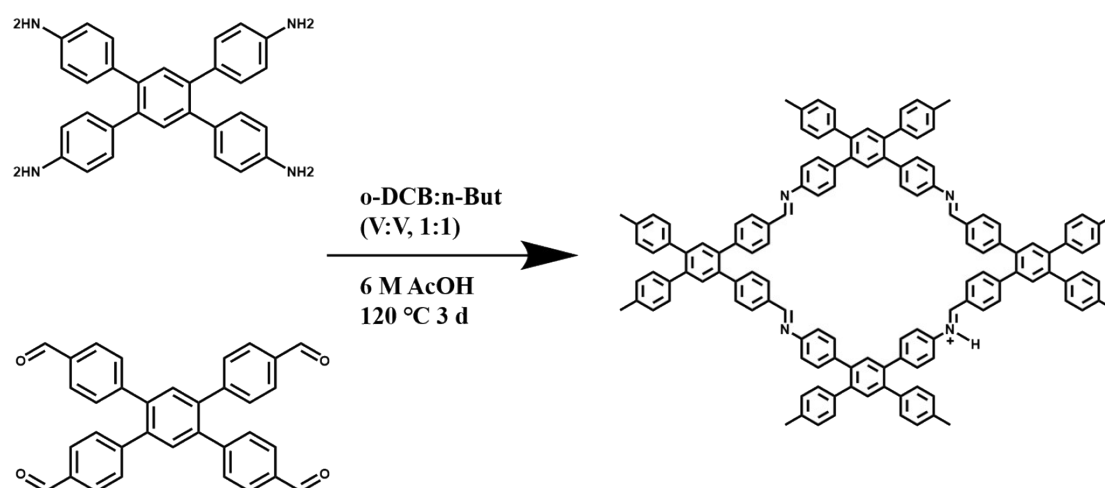
1.5 Synthetic procedures

Py-COF: A Pyrex tube was charged with Py-NH₂ (31.1 mg, 0.05 mmol), Py-CHO (28.4 mg, 0.05 mmol), *o*-1,2-Dichlorobenzene (1.4 mL), *n*-Butanol (0.6 mL), and 12 M Acetic acid (0.1 mL). This mixture was homogenized by sonication for 10 minutes and the tube was then flash frozen at 77 K (liquid N₂ bath) and degassed by three freeze-pump-thaw cycles and evacuated to an internal pressure of 100 m Torr. The tube was sealed off and then heated at 120 °C for 3 days. The brown precipitate was collected by centrifugation and washed with Tetrahydrofuran (100 mL) and anhydrous acetone (200 mL). After freeze-drying, the product was obtained an Orange powder (48 mg, 80%).

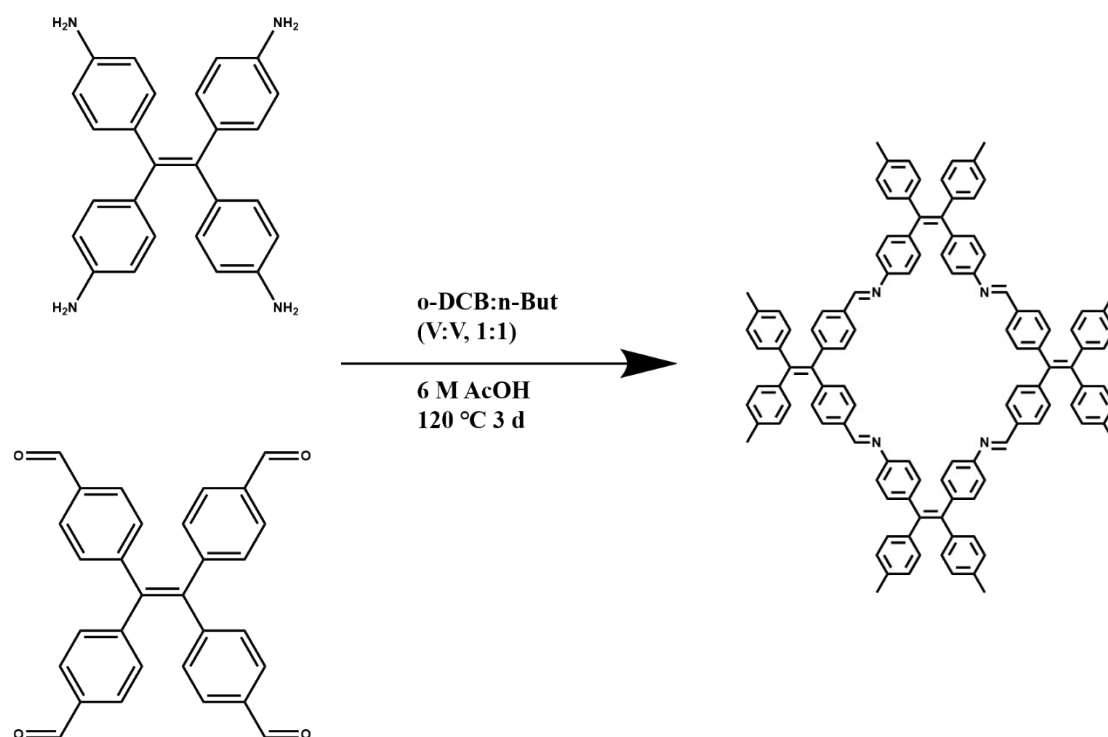


Tet-COF: A Pyrex tube was charged with 1,2,4,5-Tetrakis-(4-formylphenyl)benzene

(Tet-CHO) (25.0 mg, 0.05 mmol), 4',5'-bis(4-aminophenyl)-[1,1':2',1''-terphenyl]-4,4''-diamine (Tet-NH₂) (22.1 mg, 0.05 mmol), *o*-1,2-Dichlorobenzene (1 mL), *n*-Butanol (1 mL), and 6 M Acetic acid (0.1 mL). This mixture was homogenized by sonication for 10 minutes and the tube was then flash frozen at 77 K (liquid N₂ bath) and degassed by three freeze-pump-thaw cycles and evacuated to an internal pressure of 100 m Torr. The tube was sealed off and then heated at 120 °C for 3 days. The brown precipitate was collected by centrifugation and washed with Tetrahydrofuran (100 mL) and anhydrous acetone (200 mL). After freeze-drying, the product was obtained a white powder (39 mg, 82%).



Tpe-COF: A Pyrex tube was charged with 4,4',4'',4'''-(ethene-1,1,2,2-tetra-yl)tetrabenzaldehyde (Tpe-CHO) (44.4 mg, 0.1 mmol), Tetrakis(4-aminophenyl)ethene (Tpe-NH₂) (39.2 mg, 0.1 mmol), *o*-1,2-Dichlorobenzene (1 mL), *n*-Butanol (1 mL), and 6 M Acetic acid (0.1 mL). This mixture was homogenized by sonication for 10 minutes and the tube was then flash frozen at 77 K (liquid N₂ bath) and degassed by three freeze-pump-thaw cycles and evacuated to an internal pressure of 100 m Torr. The tube was sealed off and then heated at 120 °C for 3 days. The brown precipitate was collected by centrifugation and washed with Tetrahydrofuran (100 mL) and anhydrous acetone (200 mL). After freeze-drying, the product was obtained a white powder (63.9 mg, 77%).



Py-hCOF, Tet-hCOF, TPe-hCOF: Typically, 20 mg of the pristine COF was stirred in 50 mL of 0.1 M ascorbic acid (AC) aqueous solution for 30 minutes. Then the precipitate was isolated by centrifuge and washed with deionized water at different volumes. The samples were dried overnight in the vacuum of a freeze dryer to obtain protonated COF.

1.6 AQY measurements

Apparent quantum efficiency (AQY) measurements were performed under monochromatic irradiation, generated from a 300 W Xe lamp equipped with bandpass filters

The AQY was calculated using the following equation:

$$AQY = \frac{N_e}{N_p} \times 100\% = \frac{10^9(vN_A n) \times hc}{PA\lambda} \times 100\%$$

Where, N_e is the amount of generated electron, N_p is the incident photons, v is the H_2 evolution rate ($\text{mol} \cdot \text{s}^{-1}$), N_A is Avogadro constant ($6.022 \times 10^{23} \text{ mol}^{-1}$), n is number of transferred electrons in hydrogen evolution reaction (2), h is the Planck constant ($6.626 \times 10^{-34} \text{ J} \cdot \text{s}$), c is the speed of light ($3 \times 10^8 \text{ m} \cdot \text{s}^{-1}$), P is the intensity of irradiation light ($\text{W} \cdot \text{m}^{-2}$), A is the irradiation area (m^2), t is the photoreaction time (s), λ is the wavelength of the monochromatic light (nm).

2. Results and discussion

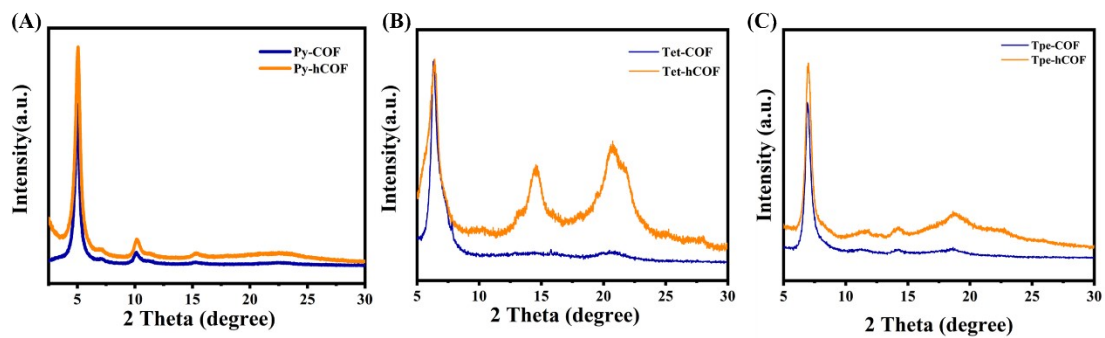


Figure S1. The experimental and protonated PXRD patterns of (A)Py-COF, (B) Tet-COF, and (C) Tpe-COF.

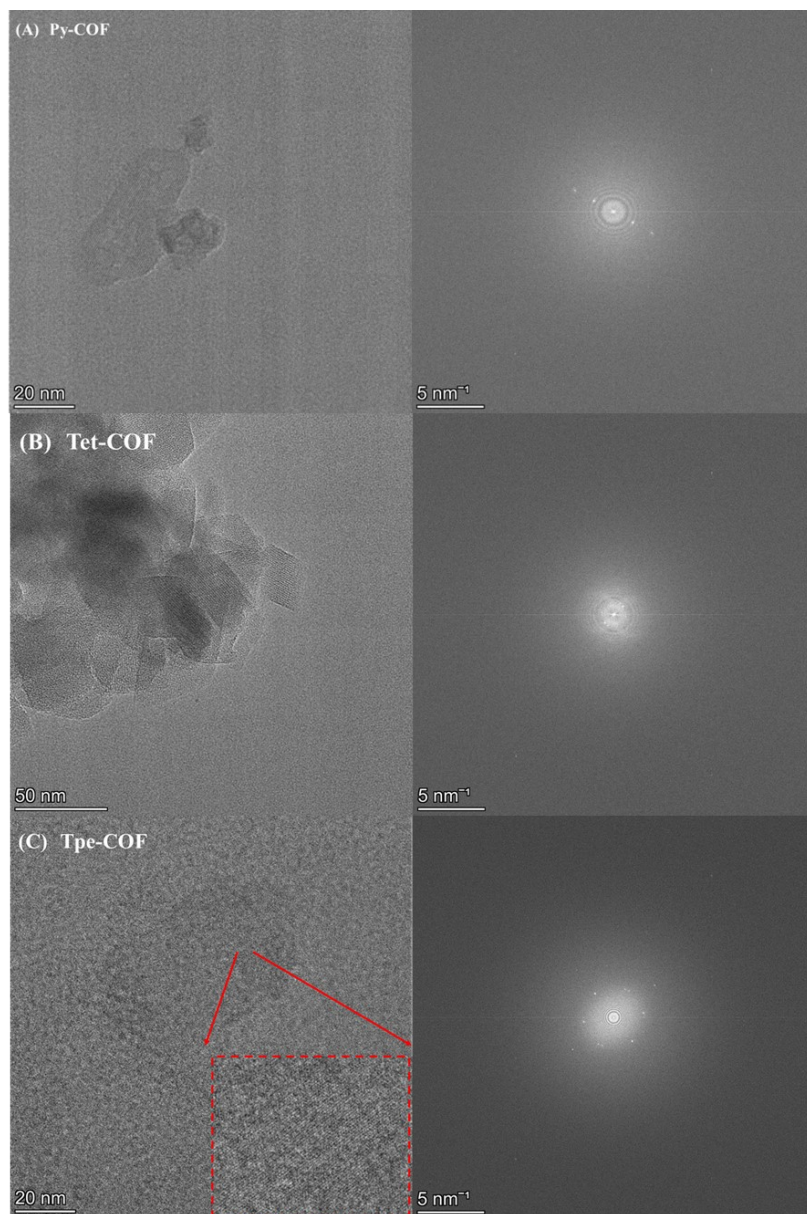


Figure S2. HR-TEM images showing lattice fringes

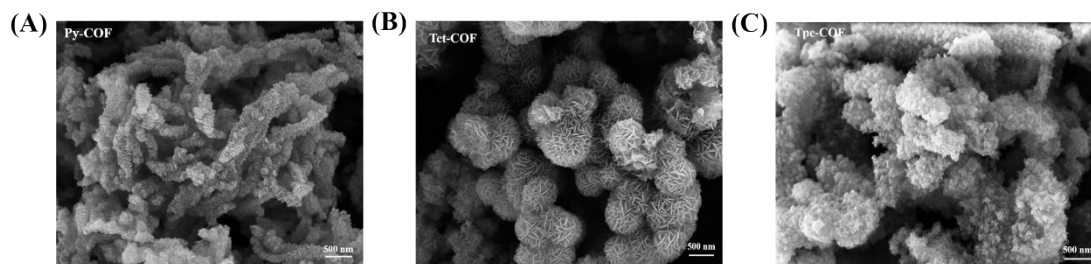


Figure S3. SEM of (A) Py-COF (B) Tpe-COF, and (C) Tpe-COF.

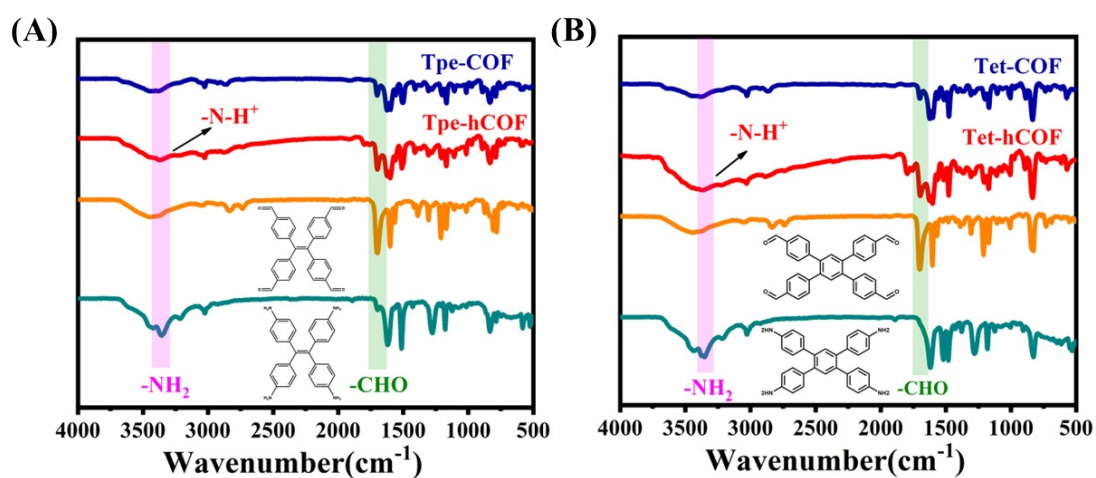


Figure S4. FT-IR spectra of (A) Tpe-COF and Tpe-hCOF, (B) Tet-COF and Tet-hCOF.

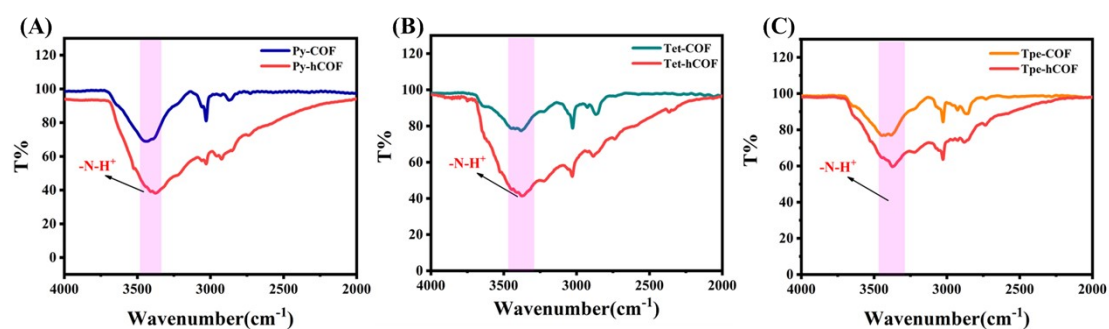


Figure S5. The infrared spectrum was amplified

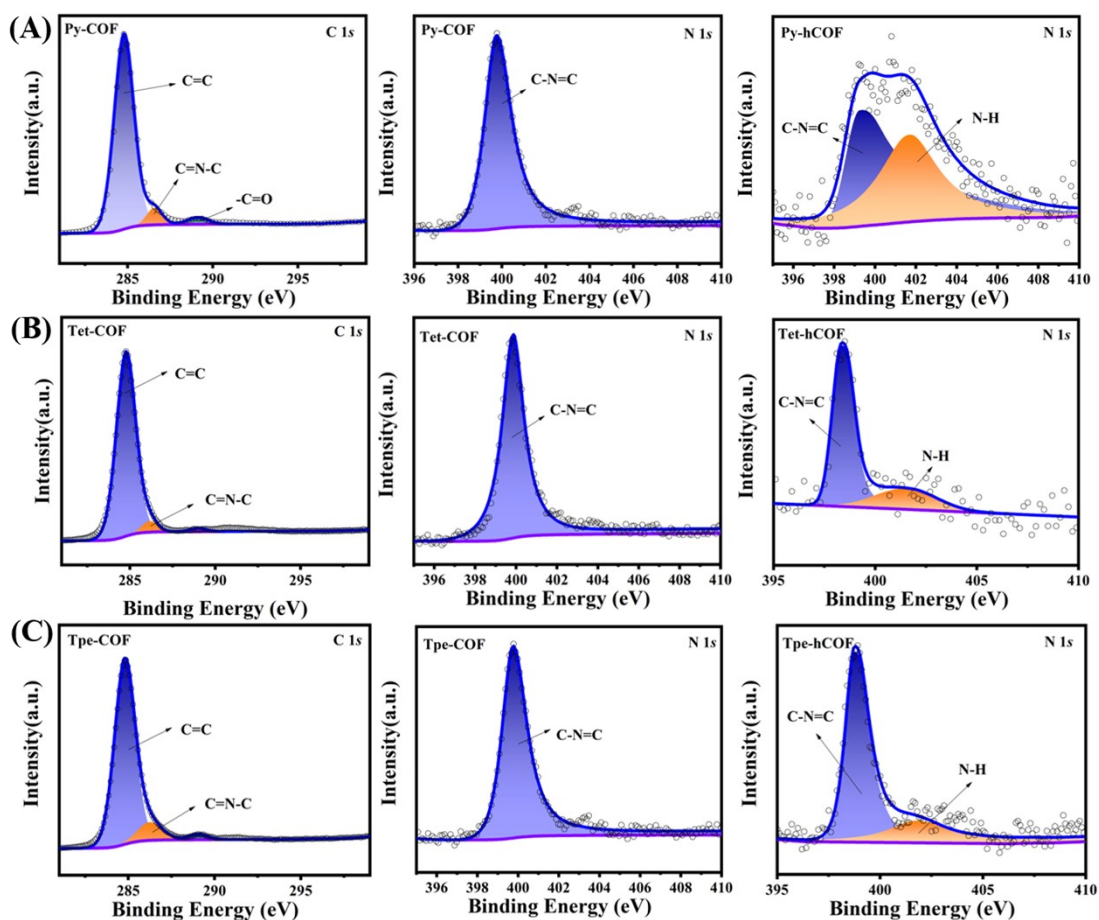


Figure S6. XPS spectra of C 1s and N 1s (A) Py-COF and Py-hCOF, (B) Tet-COF and Tet-hCOF, (C) Tpe-COF and Tpe-hCOF.

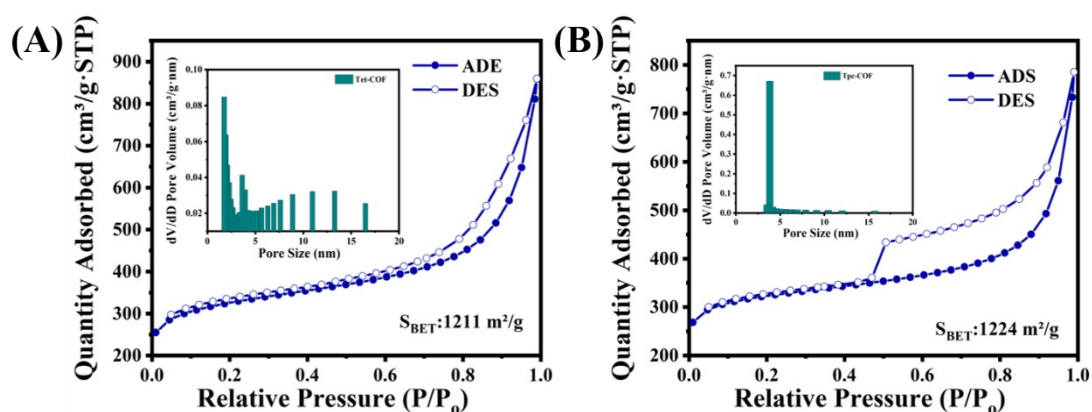


Figure S7. Nitrogen adsorption and desorption isotherms with specific surface areas: (A) Tet-COF and (B) Tpe-COF. Inset: pore diameter distribution.

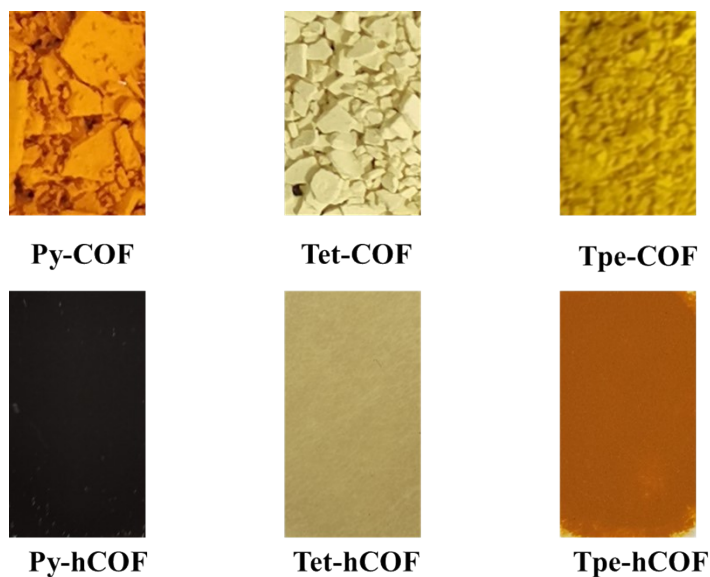


Figure S8. Comparison of COF color before and after protonation

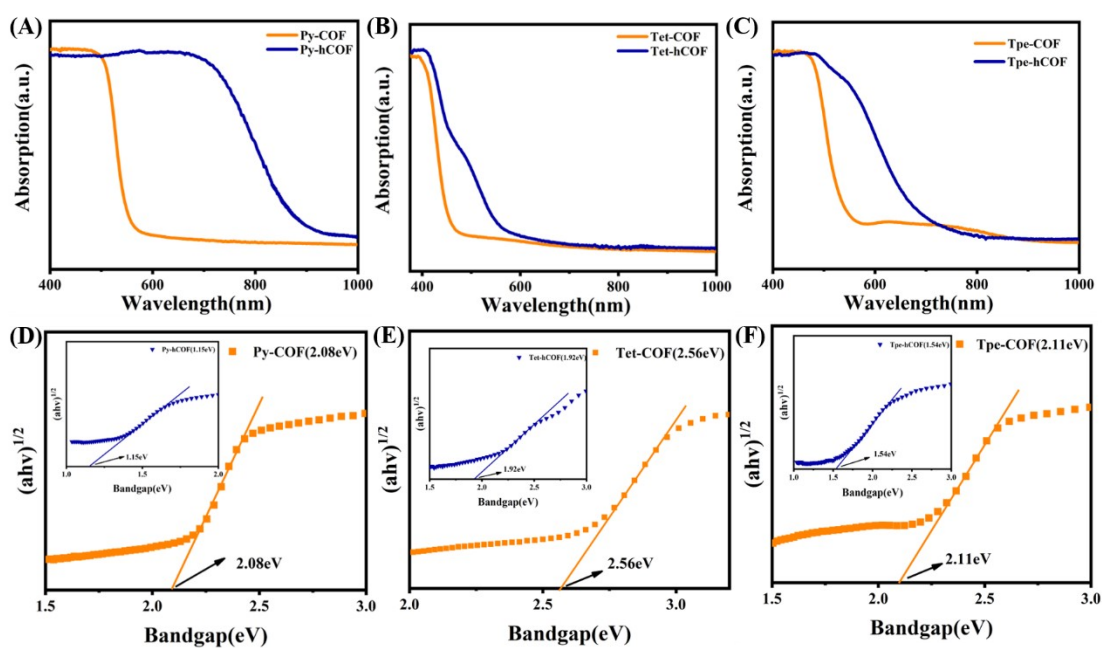


Figure S9. UV-Vis DRS spectra of COFs before and after AC treatment of (A) Py-COF, (B) Tet-COF and (C) Tpe-COF. Band structures of COFs before and after AC treatment of (D) Py-COF, (E) Tet-COF and (F) Tpe-COF.

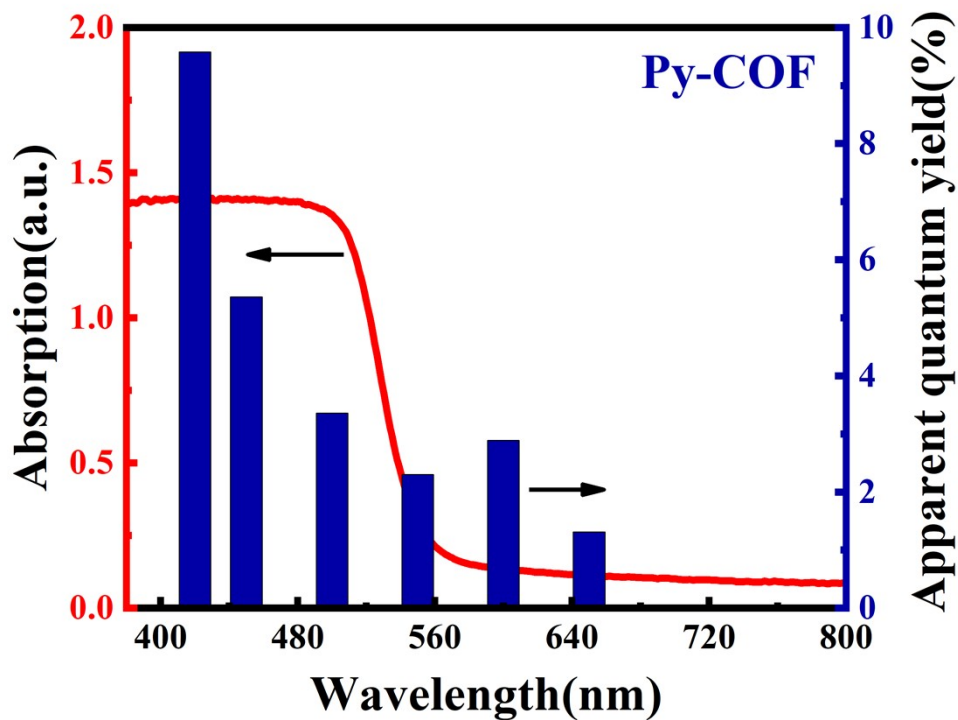


Figure S10. The apparent quantum yield (AQY) of Py-COF

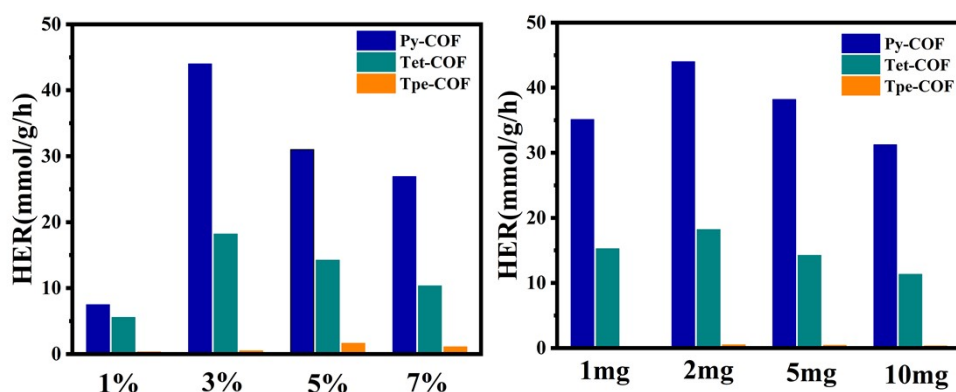


Figure S11. Photocatalytic hydrogen evolution tests with different platinum loadings and different COF qualities

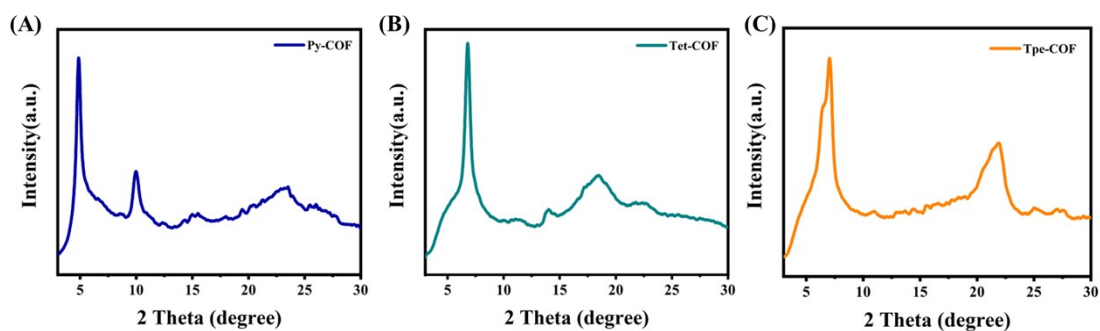


Figure S12. The XRD of COF after photocatalytic reaction

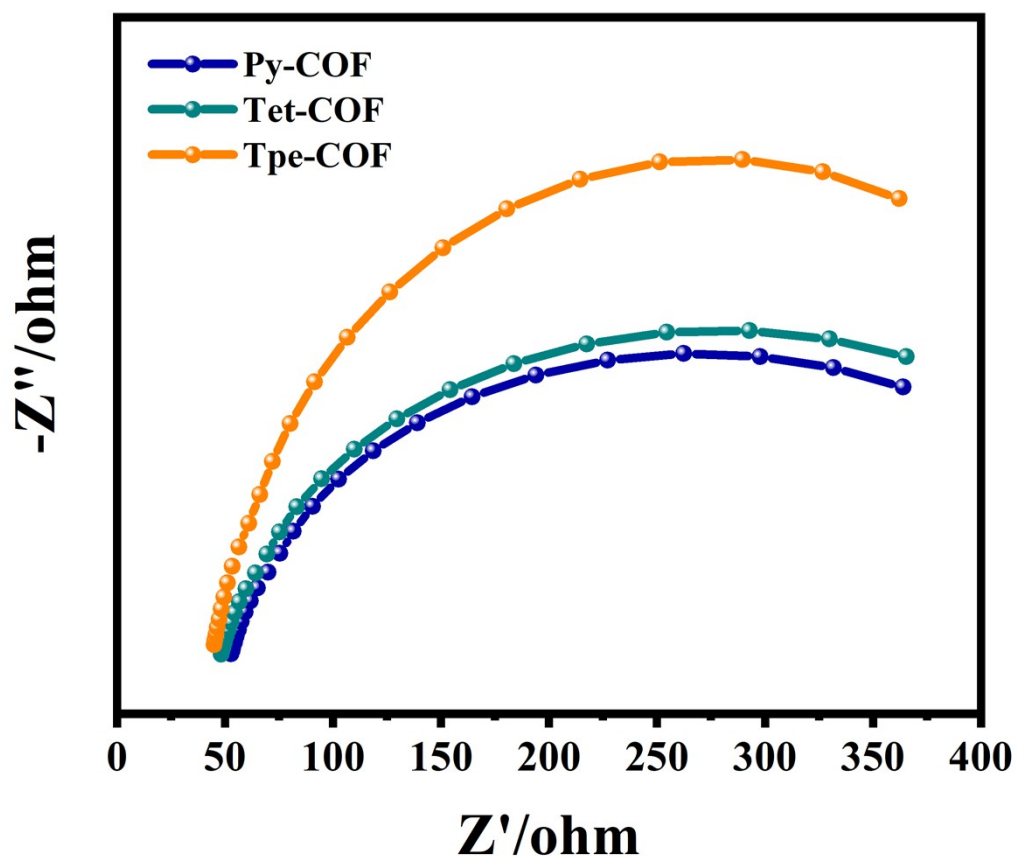


Figure S13. EIS Nyquist plots of COFs.

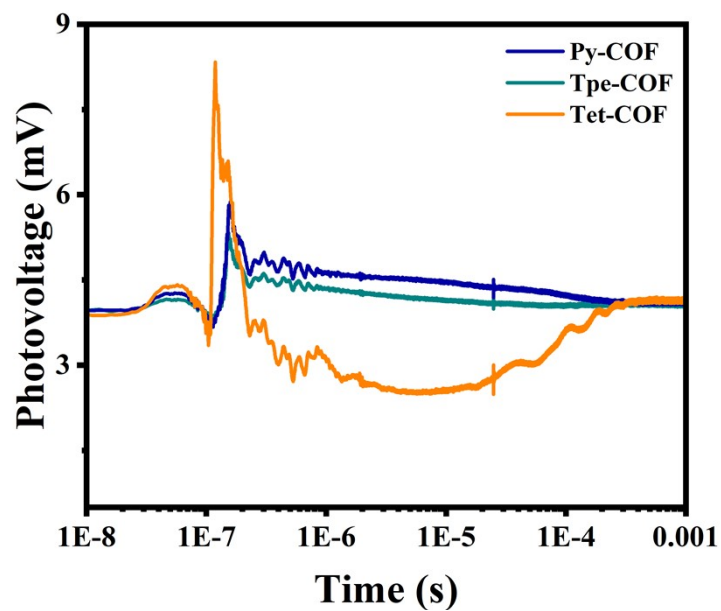


Figure S14. surface SPV of COFs.

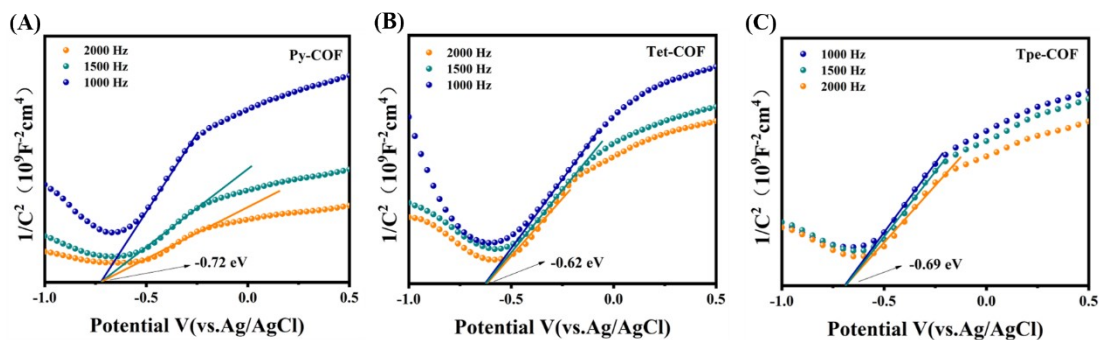


Figure S15. Mott-Schottky plots of (A) Py-COF, (B) Tet-COF, and (C) Tpe-COF

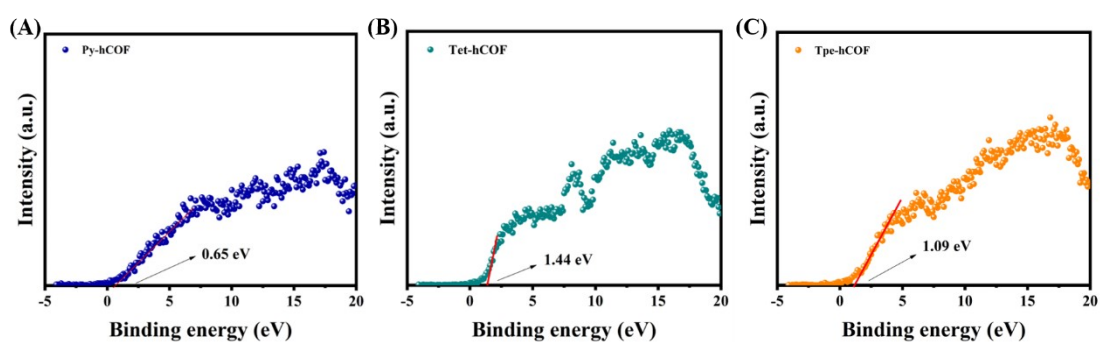


Figure S16. VB-XPS spectrum of (A) Py-hCOF, (B) Tet-hCOF and (C) Tpe-hCOF.

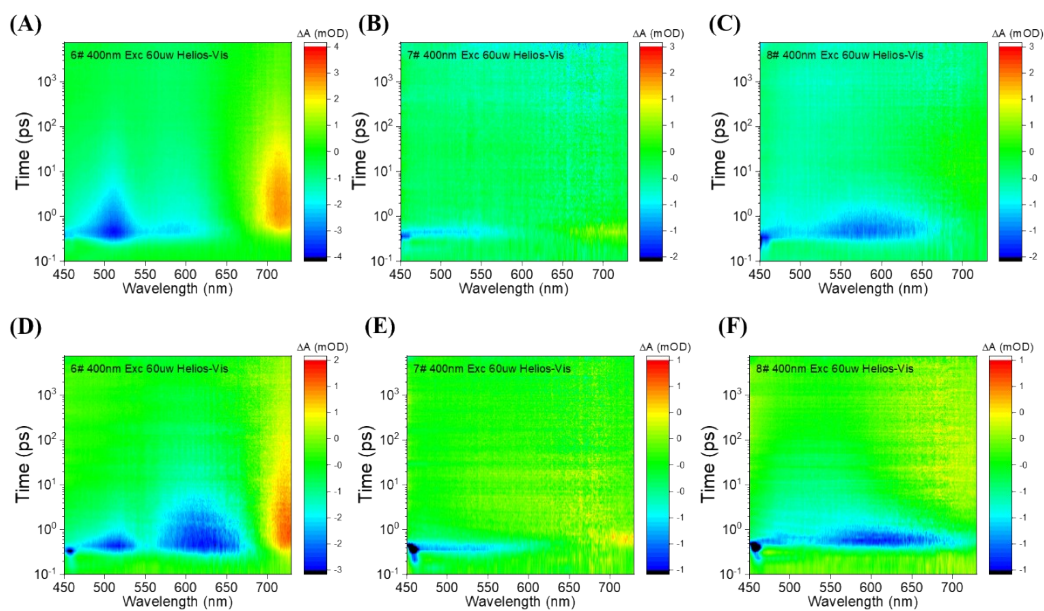


Figure S17. 2D mapping TA spectra of (A) Py-COF, (B) Tet-COF, (C) Tpe-COF in ethylene glycol. 2D mapping TA spectra of (D) Py-hCOF, (E) Tet-hCOF, (F) Tpe-hCOF in water.

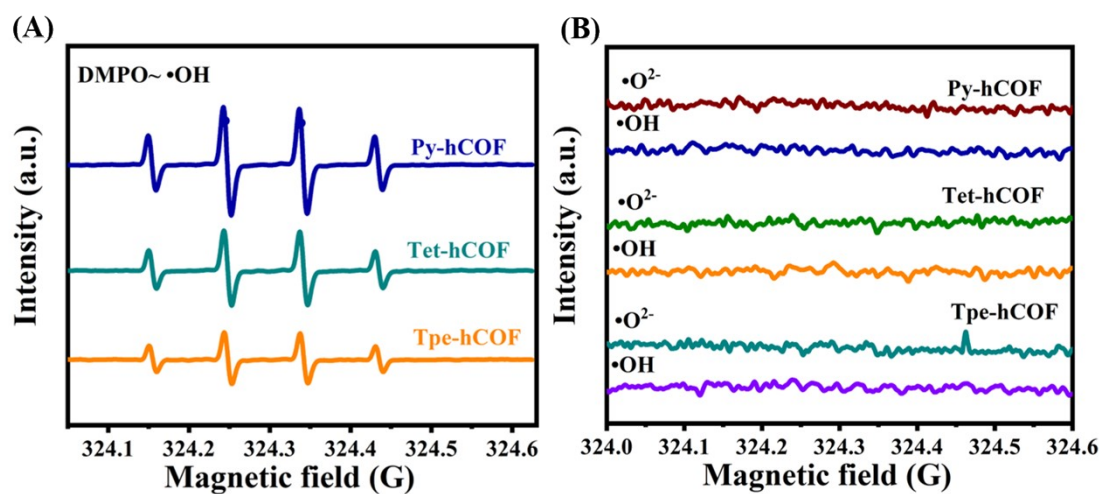


Figure S18. EPR spectra of (A) DMPO-•OH for Py-hCOF, Tet-hCOF, and Tpe-hCOF, (B) Py-hCOF, Tet-hCOF, and Tpe-hCOF in dark.

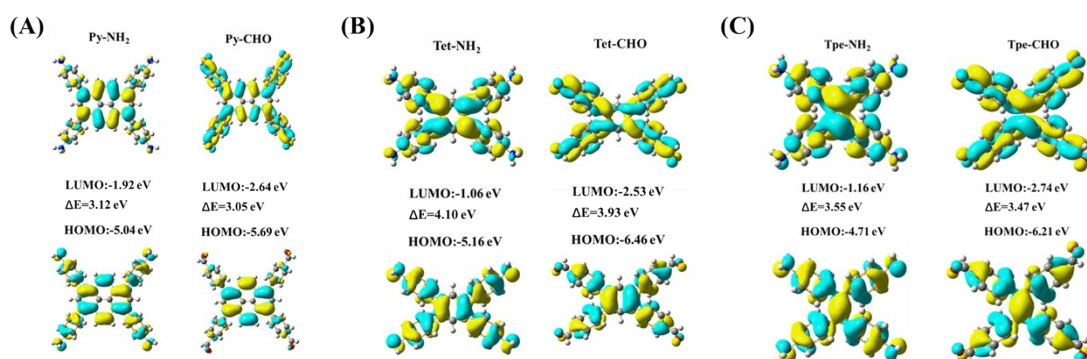


Figure S19. HOMO-LUMO of COFs monomer

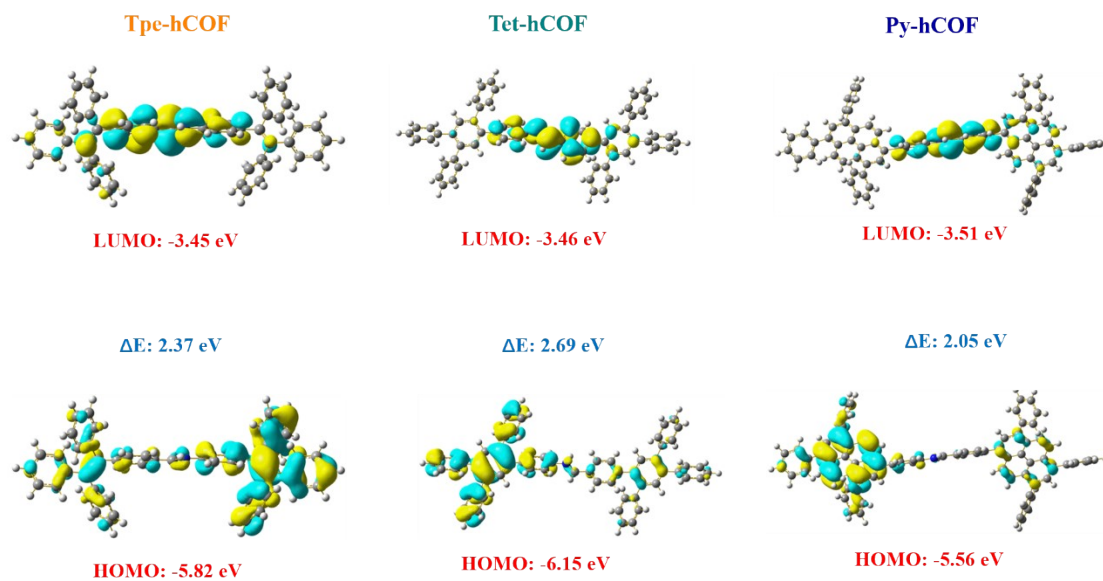


Figure S20. HOMO-LUMO of hCOFs

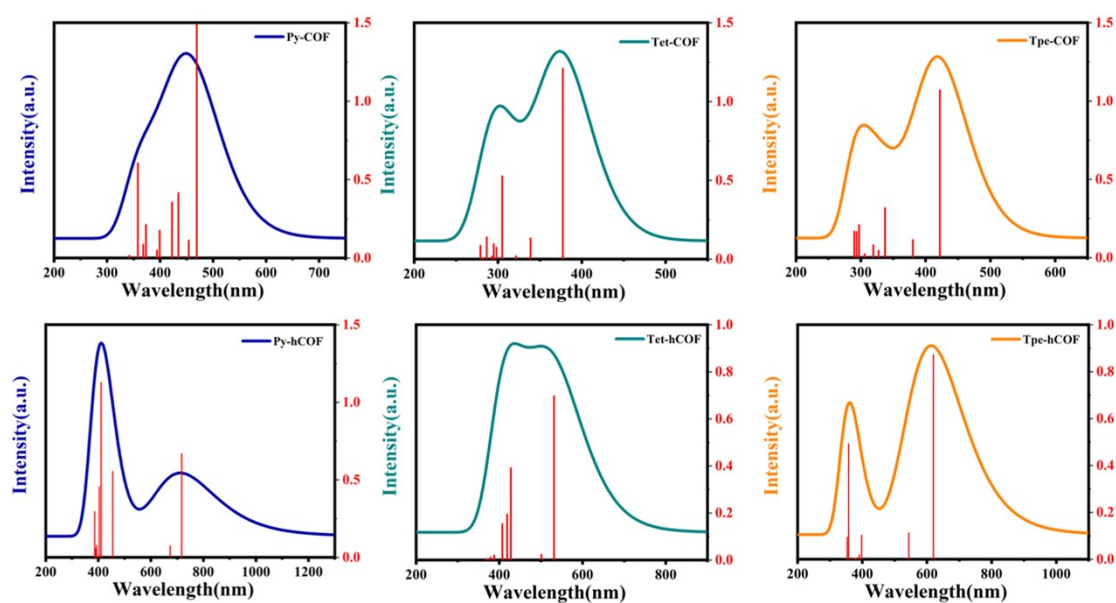


Figure S21. TD-DFT calculated fragment UV-vis absorption spectra of COFs and hCOF

Table S1. Atomistic coordinates of the simulated Py -COF.

Py-COF							
$a = 24.5268 \text{ \AA}$ $b = 26.2976 \text{ \AA}$ $c = 4.3019 \text{ \AA}$,							
$\alpha = \beta = \gamma = 90^\circ$							
space group: P222							
Atom	X	Y	Z	Atom	X	Y	Z

C1	0.55079	0.10624	0.50122	C20	0.39936	0.02579	0.51313
C2	0.55113	0.05320	0.49671	H21	0.73135	0.15045	0.83580
N3	0.74291	0.23417	0.50090	H22	0.64472	0.25196	0.17723
C4	0.69390	0.16011	0.69033	H23	0.56341	0.19346	0.17346
C5	0.69403	0.20340	0.49951	H24	0.64668	0.09541	0.86733
C6	0.64608	0.21559	0.32130	H25	0.85906	0.45283	0.52004
C7	0.60056	0.18350	0.32070	H26	0.92924	0.30252	0.74427
C8	0.60099	0.13896	0.50278	H27	0.84352	0.24823	0.67618
C9	0.64738	0.12901	0.69995	H28	0.77458	0.35983	0.01810
C10	0.94903	0.44682	0.49131	H29	0.86282	0.41142	0.06078
C11	0.94945	0.39381	0.47343	H30	0.72109	0.28410	0.13268
C12	0.89943	0.47413	0.50371	H31	0.35909	0.04688	0.54321
C13	0.89916	0.36207	0.42595	C32	0.50000	0.02665	0.50000
C14	0.89476	0.31571	0.58591	C33	0.50000	0.13077	0.50000
C15	0.84756	0.28600	0.54820	H34	0.50000	0.17407	0.50000
C16	0.80362	0.30210	0.35016	C35	0.00000	0.52664	0.50000
C17	0.80888	0.34710	0.17914	C36	0.00000	0.63098	0.50000
C18	0.85673	0.37598	0.20939	H37	0.00000	0.67429	0.50000
C19	0.75218	0.27282	0.31721	□	□	□	□

Table S2. Atomistic coordinates of the simulated Tet-COF.

Tet-COF							
$a = 24.5584 \text{ \AA}$, $b = 16.3974 \text{ \AA}$, $c = 4.5081 \text{ \AA}$,							
$\alpha = \beta = \gamma = 90^\circ$							
space group: P222							
Atom	X	Y	Z	Atom	X	Y	Z
C1	0.5490	0.0430	0.4937	C16	0.7630	0.2668	0.2295
N2	0.7461	0.2186	0.4335	H17	0.7255	0.0999	0.7939
C3	0.6898	0.1171	0.6449	H18	0.6540	0.2580	0.1158
C4	0.6950	0.1798	0.4445	H19	0.5655	0.1793	0.1514
C5	0.6504	0.2035	0.2718	H20	0.6383	0.0248	0.8357
C6	0.6020	0.1604	0.2918	H21	0.9361	0.2957	0.6423
C7	0.5980	0.0940	0.4841	H22	0.8535	0.2104	0.5200
C8	0.6418	0.0757	0.6645	H23	0.7814	0.4168	0.0495
C9	0.9508	0.4569	0.4893	H24	0.8606	0.5039	0.2083
C10	0.9027	0.4054	0.4287	H25	0.7394	0.2760	0.0140
C11	0.9007	0.3237	0.5141	C26	0.5000	0.0836	0.5000
C12	0.8557	0.2766	0.4435	H27	0.5000	0.1531	0.5000
C13	0.8132	0.3100	0.2786	C28	0.0000	0.5831	0.5000
C14	0.8156	0.3898	0.1898	H29	0.0000	0.6526	0.5000
C15	0.8592	0.4365	0.2709	□	□	□	□

Table S3. Atomistic coordinates of the simulated Tpe-COF.

Tpe-COF							
$a = 22.9779 \text{ \AA}$ $b = 15.8421 \text{ \AA}$, $c = 5.1902 \text{ \AA}$,							
$\alpha = \beta = \gamma = 90^\circ$							
space group: P222							
Atom	X	Y	Z	Atom	X	Y	Z
N1	0.7374	4.2231	8.5366	C14	0.7599	1.2810	0.3825
C2	0.6632	4.1175	8.6968	H15	0.6978	4.0980	8.8358
C3	0.6765	4.1831	8.5233	H16	0.6369	4.2569	8.2079
C4	0.6297	4.2063	8.3453	H17	0.5377	4.1815	8.2004
C5	0.5721	4.1633	8.3416	H18	0.5990	4.0224	8.8163
C6	0.5599	4.0955	8.5123	H19	0.9590	4.3084	10.7566
C7	0.6062	4.0748	8.6903	H20	0.8577	4.2359	10.7141
C8	0.9402	4.4045	10.4676	H21	0.8049	4.4165	10.1297
C9	0.9260	4.3317	10.6165	H22	0.9026	4.4901	10.1918
C10	0.8677	4.2904	10.5933	H23	0.7322	1.3043	0.2242
C11	0.8229	4.3200	10.4165	C24	0.5000	1.0446	0.5000
C12	0.8381	4.3909	10.2654	C25	1.0000	1.5448	0.5000
C13	0.8951	4.4321	10.2933	□	□	□	□

Table S4. Calculated molecular orbital at different excited states for Tpe-COF.

Model	Excitation	MOT	nm	f
Tpe-COF	S0→S1	HOMO→LUMO	422 nm	1.0695

Table S5. Calculated molecular orbital at different excited states for Tet-COF.

Model	Excitation	MOT	nm	f
Tet-COF	S0→S1	HOMO-2→LUMO	377 nm	1.2098
		HOMO-1→LUMO		

Table S6. Calculated molecular orbital at different excited states for Py-COF.

Model	Excitation	MOT	nm	f
Py-COF	S0→S1	HOMO-1→LUMO	469 nm	1.4868
		HOMO-1→LUMO+1		
		HOMO→LUMO		
		HOMO→LUMO+2		

Table S7. The calculated value of the ultraviolet absorption of the excited state S1 after protonation.

Model	Pre-protonation	Post-protonation	Differentials
Py-COF	469 nm	783 nm	314
Tet-COF	377 nm	555 nm	178
Tpe-COF	422 nm	641 nm	219

References

1. T. Lu and F. Chen, Multiwfn: A multifunctional wavefunction analyzer, *Journal of Computational Chemistry*, 2012, **33**, 580-592.
2. P. ChacÃ³n, F. Tama and W. Wriggers, Mega-Dalton Biomolecular Motion Captured from Electron Microscopy Reconstructions, *Journal of Molecular Biology*, 2003, **326**, 485-492.